Communication

3 W Continuous-Wave Room Temperature Quantum Cascade Laser Grown by Metal-Organic Chemical Vapor Deposition

Teng Fei [1], Shenqiang Zhai [1,*], Jinchuan Zhang [1,*], Quanyong Lu [2], Ning Zhuo [1], Junqi Liu [1,3], Lijun Wang [1,3], Shuman Liu [1,3], Zhiwei Jia [1], Kun Li [1], Yongqiang Sun [1], Kai Guo [1] and Fengqi Liu [1,3]

[1] Key Laboratory of Semiconductor Materials Science, Institute of Semiconductors, Chinese Academy of Sciences, Beijing Key Laboratory of Low Dimensional Semiconductor Materials and Devices, Beijing 100083, China
[2] Beijing Academy of Quantum Information Sciences, Beijing 100193, China
[3] Center of Materials Science and Optoelectronics Engineering, University of Chinese Academy of Sciences, Beijing 100049, China
* Correspondence: zsqlzsmbj@semi.ac.cn (S.Z.); zhangjinchuan@semi.ac.cn (J.Z.)

Abstract: In this article, we report a high-performance λ ~ 4.6 μm quantum cascade laser grown by metal-organic chemical vapor deposition. Continuous wave power of 3 W was obtained from an 8 mm-long and 7.5 μm wide coated laser at 285 K. The maximum pulsed and CW wall-plug efficiency reached 15.4% and 10.4%, respectively. The device performance shows the great potential of metal-organic chemical vapor deposition growth for quantum cascade material and devices.

Keywords: quantum cascade laser; metal-organic chemical vapor deposition; high power

Citation: Fei, T.; Zhai, S.; Zhang, J.; Lu, Q.; Zhuo, N.; Liu, J.; Wang, L.; Liu, S.; Jia, Z.; Li, K.; et al. 3 W Continuous-Wave Room Temperature Quantum Cascade Laser Grown by Metal-Organic Chemical Vapor Deposition. *Photonics* **2023**, *10*, 47. https://doi.org/10.3390/photonics10010047

Received: 16 November 2022
Revised: 27 December 2022
Accepted: 28 December 2022
Published: 3 January 2023

Copyright: © 2023 by the authors. Licensee MDPI, Basel, Switzerland. This article is an open access article distributed under the terms and conditions of the Creative Commons Attribution (CC BY) license (https://creativecommons.org/licenses/by/4.0/).

1. Introduction

In the mid-infrared region, quantum cascade lasers [1] (QCL) has proven to be a powerful and versatile light source owing to their advantages in practicality including high power, wide tunability, small size and easy operation. In recent years, great efforts have been devoted to developing device performance, in terms of low power consumption [2–4], high efficiency [5–9] and high power [10,11]. The increasing demands of infrared countermeasures and the rapid development in long-range free-space communication [12,13] have served as major drivers to improve the power of quantum cascade lasers.

Since the first demonstration of QCL, molecular beam epitaxy (MBE) has mainly been used for the growth of QCL cores [14,15]. The precise control of layer thickness and the sharp interface in MBE are essential for the growth of ultrathin QCL layers. Previous efforts have focused on practically important λ ~ 4.6 μm QCLs to avoid atmospheric absorption. Room temperature watt-level power has been achieved so far. In particular, more than 3 W output power from a single facet was independently presented by two groups [16–18]. However, the cost of high-power QCLs chips is several orders of magnitude higher than that of near-infrared semiconductor laser chips, in part due to the high cost of the molecular beam epitaxy process [19]. Metal-organic chemical vapor deposition (MOCVD) is a well-established technique to grow an optoelectronic structure in the industrial field. It has the advantage of excellent uniformity and repeatability, but still poses challenges with respect to the growth of QCL cores. Significant research has been made to improve the performance of MOCVD-gown QCLs in the past two decades [20–23]. In 2010, Yu Yao reported a continuum-to-continuum design. The reported room temperature power and WPE reached 5 W and 23% in pulsed mode [24], which are comparable to the state-of-the-art MBE-grown QCLs. However, the CW power dropped rapidly to only 1 W at room temperature due to severe carrier leakage and backfilling. Most recently, record high power of 2.6 W emitting at λ ~5 μm at 288 K have been demonstrated [7] by employing a variety of active region materials of different compositions to suppress carrier leakage. However,

the promotion of device performance comes at the cost of increasing growth difficulty. The adopted 11 different compositions place higher requirements on material growth, which also limits the efficiency of epitaxial growth. Despite the aforementioned achievements, the power of MOCVD-grown QCLs is still less than MBE-grown QCLs. This is mainly because the MBE system adopts an ultra-high vacuum environment, in which the interface switching speed is fast. In addition, the concentration of background impurities is low. In contrast, in the MOCVD system, the source gas flow is inevitably delayed during the interface switching process [25]. A smoother interface and lower background impurities contribute to the low interface roughness and low optical loss in MBE-grown QCLs [17]. However, we believe it is possible to obtain considerable high-quality material for MOCVD-grown QCLs. We have recently achieved high-quality long-wave MOCVD-grown QCL by carefully optimizing the growth conditions, particularly the growth interface [6]. QCLs emitting at λ ~8.5 μm with a record high efficiency of 7.1% and 1 W CW power at room temperature were demonstrated. Here, we follow our previous method and extend the wavelength to the mid-wavelength. Combined with the dedicated energy band design, it is reasonable to speculate that the performance of mid-wave MOCVD-grown QCLs can be further improved.

In this paper, we report the growth and fabrication of 4.6 μm strain-balanced $In_{0.66}Ga_{0.34}As$/$In_{0.36}Al_{0.64}As$ using low-pressure MOCVD. Based on the slightly diagonal single phonon resonance design, a high-quality quantum cascade structure was obtained. An 8 mm-long, 7.5 μm-wide device was capable of delivering 5.8 W peak power in pulse mode (500 ns/2%) at 285 K. The threshold current density, slope efficiency and maximum WPE were 1.5 kA/cm^2, 4.35 W/A and 15.4%, respectively. The CW power of the device reaches 3 W at 285 K with a maximum WPE of 10.4%.

2. Materials and Methods

The laser core consisted of 40 periods of strain-balanced InGaAs/InAlAs quantum well and barrier pairs based on the single phonon resonance (SPR) design similar to the structure in Ref [26]. For the reference design, the upper lasing state is highly localized in the first thin well, which enhances the coupling between the injector region and the upper lasing state [14,27]. In addition, the optical transition is slightly diagonal, which increases the lifetime of the upper state. Figure 1 shows a comparison between the reference design and the one optimized. The thickness of the active region was slightly modified to target the wavelength of 4.5μm. In addition, the compositions of Al in InAlAs and Ga in InGaAs were changed to 0.64 and 0.34, respectively. As a result, the conduction band offset was increased from 708 meV to 782 meV. Therefore, thermally activated leakage of electrons from the upper laser level into the continuum can be suppressed. Another notable feature is the increased energy difference between the upper lasing state (E_4) and the excited state (E_5). The calculated energy difference E_{54} is increased from 70 to 91 meV.

The QCL structure presented in this article was grown on a 2-inch n-InP substrate (S, 2E18) using a low-pressure (100 mbar) MOCVD with a close-coupled showerhead (3 × 2″) reactor. The group III precursors were trimethylindium (TMIn), trimethylgallium (TMGa), and trimethylaluminum (TMAl). The group V precursors were purified arsine (AsH_3) and phosphine (PH_3). Silane (SiH_4, 0.02% in H_2) was used as the n-type dopant. The total flow rate was 8 L/min. The growth temperature was read using a thermocouple mounted under the graphite disk. Before growth, the InP(S, 2E18) substrates were loaded into the chamber and deoxidized at 760 °C for 5 min in PH_3 ambient. The growth was initiated by the deposition of a 500 nm InP buffer layer followed by a 3 μm n-InP (4E16) lower waveguide at 700 °C. Then, the temperature was increased to 720 °C to grow the InGaAs/InAlAs laser core region. There were no growth interrupts at the interfaces of InGaAs-to-InAlAs and InAlAs-to-InGaAs. The TMIn flow rate was kept constant during InGaAs and InAlAs growth. Then, the temperature was decreased to 700 °C to grow a 3 μm InP upper waveguide (4E16) which was covered by a 1 μm InP cap layer (2E18).

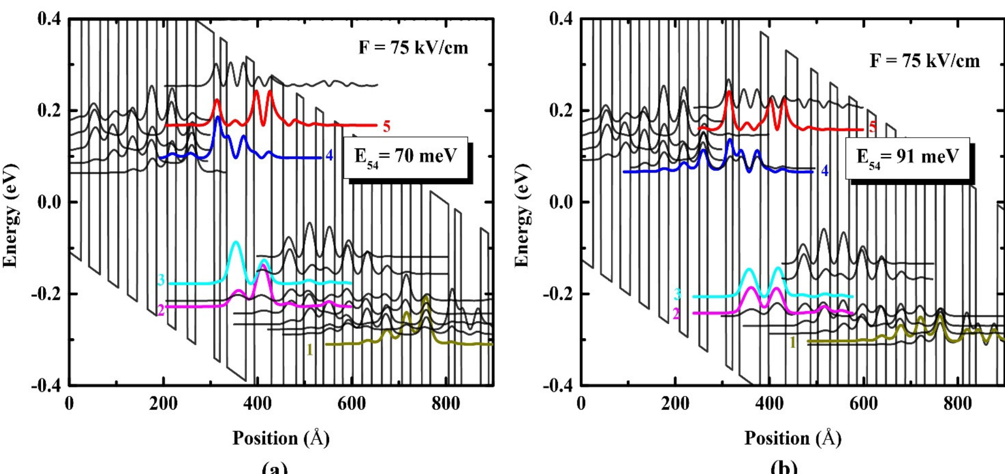

Figure 1. Band diagrams of the referenced (**a**) and modified (**b**) designs at 75 kV/cm electric field. The energy states marked with different colors are the excited state (E_5), the upper state (E_4), the lower state (E_3), the extracted state (E_2) and the injected state (E_1).

Once the wafer growth was achieved, the material was characterized by high-resolution X-ray diffraction (HRXRD) and atomic force microscopy (AFM) to investigate the material quality. Figure 2a compares the measured and simulated HRXRD results. The experimental result is almost fully in line with the simulated one. Multiple high-order satellite peaks can be clearly observed, with extremely sharp and narrow FWHM of about 15 arc seconds. The observation of multiple satellite peaks at HRXRD indicates excellent in-plane uniformity in terms of layer thickness and chemical composition. To characterize the surface morphology of QCL, one piece of the wafer was etched by HCl to remove the upper InP waveguide. Figure 2b shows the surface image of the active core characterized by AFM (5 µm × 5 µm scan in contact mode). It can be seen that for such hundreds of strained quantum well/barrier pairs, step-flow growth is still achieved. The calculated surface root-mean-square (RMS) is only 0.15 nm. The average distance between different steps is 0.25 µm.

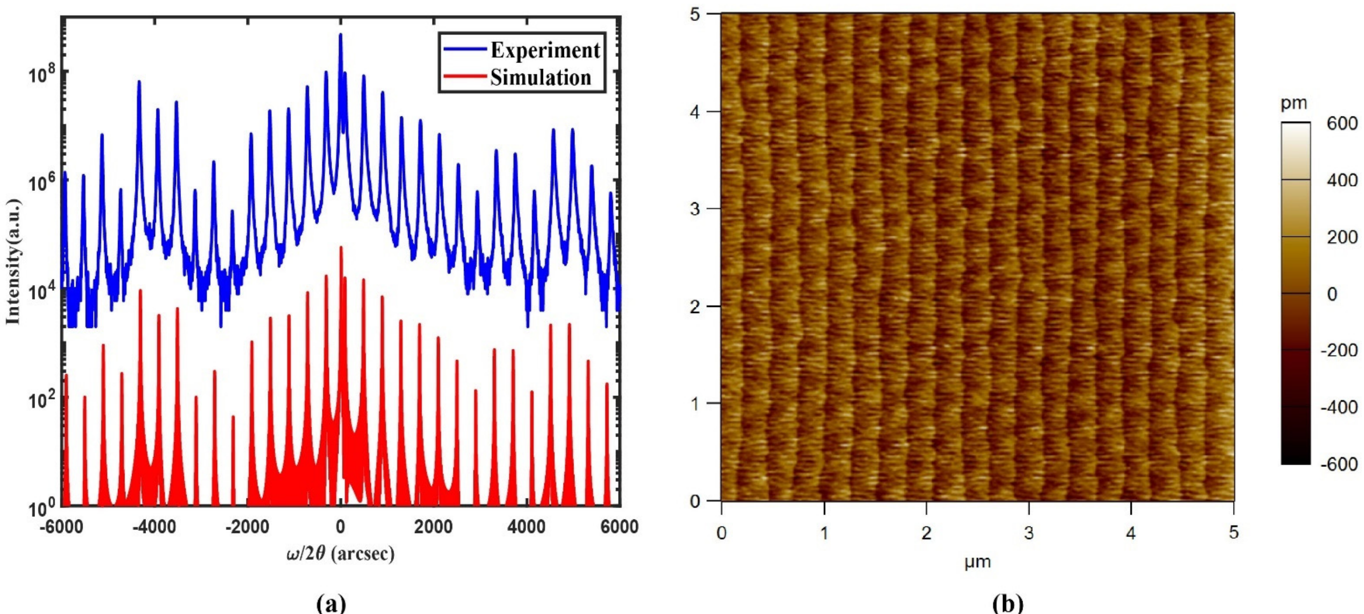

Figure 2. (**a**) High-resolution XRD of experimental (blue, upper curve) and simulated (red, lower curve) results of strain-balanced QCL structures. (**b**) Atomic force microscopy image (5 × 5 µm) of 40-period strain-balanced QCL structures.

The fabrication process of QCLs is as follows. One piece of the wafer was processed into a double-channel geometry with a ridge of 16 μm to characterize the intrinsic physical parameters of the wafer, for example, waveguide loss and modal differential gain. Another piece of the wafer was processed into a buried hetero-structure (BH) configuration with a ridge width of 7.5 μm as shown in the Appendix A, Figure A1. Firstly, the wafer was patterned into stripes by using a 300 nm-thick SiO_2 mask and wet-etched through the active region into a double-channel geometry. The etchant is HBr:HNO_3:H_2O (1:1:10) which is nonselective and isotropic. After etching and rinsing, Fe-doped semi-insulating InP was selective-area regrown by MOCVD to planarize the channels. Then a SiO_2 mask was removed using a buffered oxide etch (BOE), and a new 300 nm-thick SiO_2 layer was deposited by plasma-enhanced chemical vapor deposition as an electrical isolation layer. The current injection windows were opened on the top of the ridge by lithography. Besides, top contact was made, including a Ti/Au layer by e-beam evaporation and a 5 μm-thick Au layer by electroplating. The backside of the wafer was thinned down to 120 μm and polished. An AuGeNi/Au layer was then evaporated as the bottom contact. The processed wafer was annealed at 370 °C and cleaved into 8 mm bars. A high-reflectivity coating was applied on the back facet with the front facet left uncoated. For packaging, the chips were soldered epi-down on diamond submounts to improve the heat removal efficiency. Then the submounts with chips were mounted on the copper heat sinks with indium solder followed by wire bonding.

3. Results and Discussion

After device fabrication, testing was conducted by fixing the laser on a water-cooling platform with a chip facet close to a calibrated thermopile detector. For pulsed measurements, the voltage and pulsed width were measured using a voltage probe. The peak power in pulsed operation (pulse width 500 ns, repetition 40 kHz) was calculated by dividing average power by duty cycle (2%). The temperature was monitored by a thermistor and controlled by a thermoelectric cooler (TEC). Figure 3a shows the pulsed power-current-voltage (PIV) curves of QCL devices with 16-μm-wide and 2-, 4-, and 6-mm-long cavities. The heat sink temperature is kept at 295 K. Figure 3b shows the threshold current density dependence on mirror loss and inverse external quantum efficiency dependence on inverse mirror loss. The internal quantum efficiency, waveguide loss, transparency current density and differential gain were determined to be 60%, 0.66 cm^{-1}, 1.5 kA/cm^2 and 7.24 cm/kA. The waveguide loss is three times smaller than in Ref [7], which means a loss in slope efficiency can be negligible when the length is increased. Therefore, we can use longer cavities to achieve better performance. However, this waveguide loss is slightly larger than that of the state-of-the-art MBE-grown QCLs [8], implying that there is still room for improvement in material quality. In addition, the modal differential gain is 2.7 times larger than that in Ref [9], which features a diagonal design. The modal gain strongly depends on the overlap between the upper laser level and the lower laser level. In diagonal designs, increasing the lifetime of the upper laser level comes at the cost of lower differential modal gain as in Ref [9]. The slightly diagonal design in this paper can increase the lifetime of the upper laser level without much compromise on the differential gain.

Figure 4 shows the CW (solid lines) and pulsed (dash lines) PIV and WPE results at 285 K. The AR-HR coated device emits to 3 W (5.8 W) with threshold current density J_{th} = 1.76 kA/cm^2 (1.5 kA/cm^2), slope efficiency η_s = 4 W/A (4.35 W/A), and WPE = 10.4% (15.4%), for CW (pulsed mode) operation. The L-I curves (red lines) show kink-free straight lines up to the saturation current, which indicates no mode hopping occurred. The inset shows the laser spectrum of the device at room temperature. The emission spectrum centered at 2160 cm^{-1} (4.6 μm) was obtained by Fourier transformed infrared spectrometer (FTIR) in rapid scan mode with a resolution of 0.25 cm^{-1}.

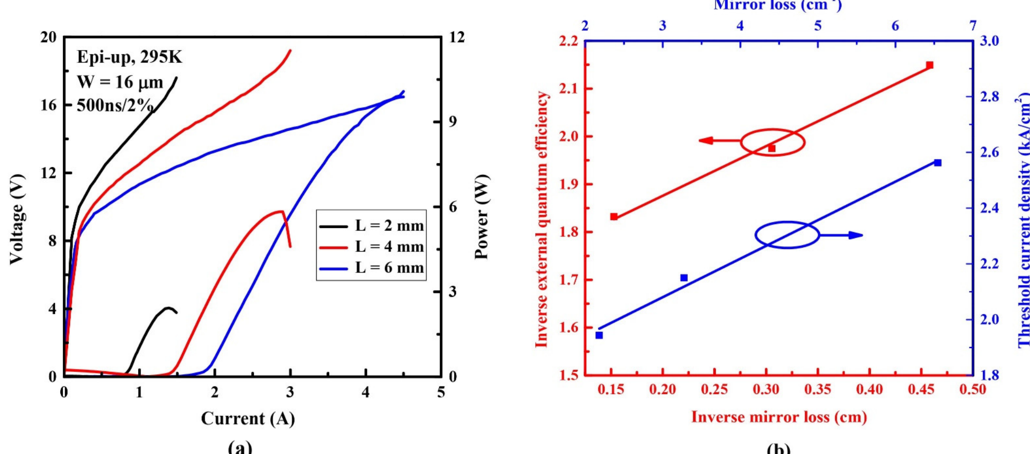

Figure 3. (**a**) the pulsed PIV curves of QCL devices with different length cavities. (**b**) threshold current density dependence on mirror loss (blue line) and inverse external quantum efficiency dependence on inverse mirror loss (red line).

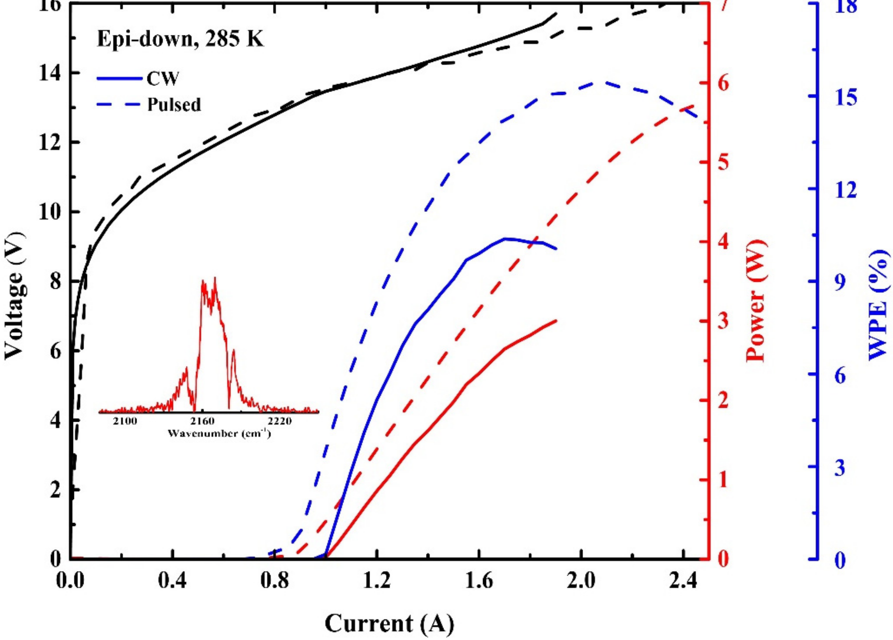

Figure 4. Continuous wave (solid lines) and pulsed (dashed lines) P-I-V and WPE characterization for a 8 mm-long and 7.5 μm-wide QCL device. The inset shows the lasing spectrum in CW mode.

Figure 5 shows the pulsed mode PIV results at different temperatures. As the temperature increases, threshold current density increases and slope efficiency decreases as expected. An experimental relationship can be established using the following equations:

$$J_{th} = J_0 \exp(T/T_0)\eta_s = \eta_0 \exp(-T/T_1)$$

where T is the heat sink temperature. The characteristic temperatures T_0 and T_1 in the pulsed operation are identified to be 240 K and 264 K, respectively. Compared with previously reported QCLs in Ref [26], T_0 and T_1 are increased by 50 K and 124 K, respectively. We attribute the increase to the larger spacing between the upper laser level and the excited state, and to the continuum. The high T_0 indicates that the thermal backfilling is significantly suppressed. Furthermore, the T_0 of this device is comparable with that of the previously reported muti-composition design QCLs in Ref [7], which features a higher E_{54}

of ~100 meV. The relatively low T_1 can be improved by reducing the overlap between the upper state E_4 and the excited state E_5, as described in Ref [9,27].

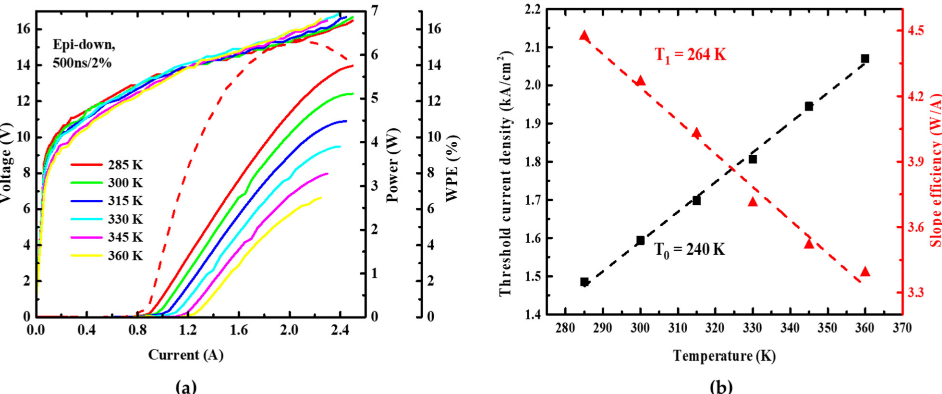

Figure 5. (**a**) Temperature-dependent P-I-V characteristics of QCL in pulsed mode. The red dash line shows the calculated WPE at 285 K. (**b**) Threshold current density and slope efficiency at different temperatures in pulse conditions at 500 ns, 2% duty cycle. The dashed lines represent exponential fits to the data.

Figure 6a shows the beam image at 1.9 A in CW operation. The transverse mode was obtained by placing a pyroelectric camera 1.5 m away from the collimated chip. The beam shape remains basically unchanged with some beam steering at the maximum current density. This beam steering results from the onset of the first-order lateral mode at a high injection current. Figure 6b shows the far field pattern at different currents. The far-field pattern was obtained by fixing the device on a motorized rotation stage with 0.1° resolution about 40 cm away from the mercury cadmium telluride detector. Furthermore, beam steering was suppressed thanks to the temperature-insensitive design [28]. In addition, we have measured the beam M^2 at 1.5 A in CW mode as shown in Appendix B, Table A1. The calculated beam M^2 in the *x*-axis and *y*-axis direction are 1.146 and 1.045.

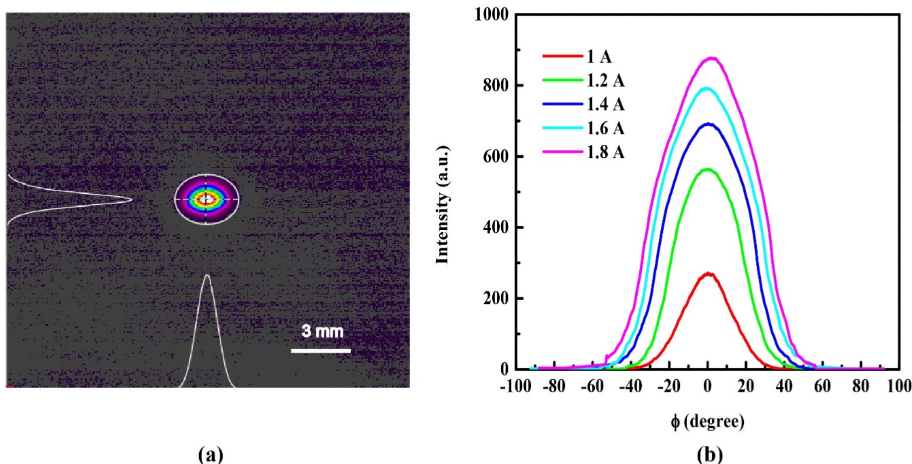

Figure 6. (**a**) The beam picture of the device at 1.9 A in CW mode at room temperature. (**b**) The far field pattern at different current in pulse mode.

In summary, we demonstrated high power 4.6 μm QCL using a single phonon resonance design. Room temperature CW power up to 3 W with a maximum WPE of 10.4% was obtained from an 8 mm-long, 7.5 μm-wide, AR-HR coated device. The device shows a characteristic that the threshold current is insensitive to temperature changes. In addition, the beam shape remains basically unchanged until the saturation current.

Author Contributions: Conceptualization, S.Z., J.Z. and T.F.; methodology, J.Z., N.Z., L.W., S.L. and T.F.; investigation, T.F., S.Z., Y.S., K.L., K.G. and Z.J.; writing—original draft preparation, T.F.; writing—review and editing, T.F., Q.L., Z.J., Y.S. and S.Z.; supervision, S.Z., J.L. and F.L. All authors have read and agreed to the published version of the manuscript.

Funding: This work was supported by the National Key Research and Development Program of China (Grant Nos. 2021YFB3201901), in part by National Natural Science Foundation of China (Grant Nos. 61991430, Grant Nos. 62274014), in part by Youth Innovation Promotion Association of the Chinese Academy of Sciences (2022112) and in part by the Key projects of the Chinese Academy of Sciences (Grant Nos. YJKYYQ20190002, Grant QYZDJ-SSW-JSC027, Grant XDB43000000, Grant ZDKYYQ20200006).

Data Availability Statement: The data presented in this study are available on reasonable request from the corresponding author.

Acknowledgments: The authors gratefully acknowledge Xiaoyu Ma from the Institute of Semiconductors, CAS for valuable discussion. We also thank Ping Liang and Fengmin Cheng for their help in device processing.

Conflicts of Interest: The authors declare no conflict of interest.

Appendix A

Figure A1 shows the scanning electron microscopy (SEM) image of laser cross-section.

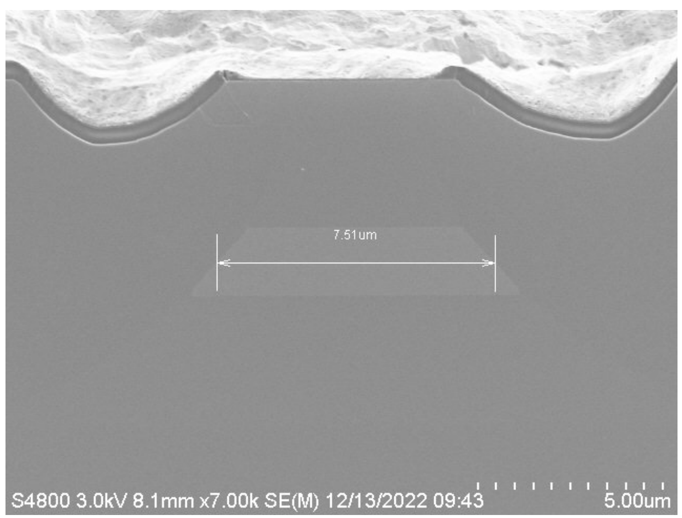

Figure A1. SEM picture of the laser cross section.

Appendix B

Table A1 shows the relation between the width of light beam and distance.

Table A1. Relation between the width of light beam and distance.

Z/mm	Dx/mm	Dy/mm
300	3.04	2.57
500	3.24	3.02
700	3.57	3.55
1100	4.60	4.92
1300	5.25	5.84
1500	6.02	6.66

The corresponding fitted beam waist diameter and beam divergence (full angle) in *X*-axis and *Y*-axis directions are as follows: D_{x0} = 3 mm, D_{y0} = 2.6 mm; θ_x = 2.1 mrad, θ_y = 2.3 mrad; M^2x = 1.146, M^2y = 1.045.

References

1. Faist, J.; Capasso, F.; Sivco, D.L.; Sirtori, C.; Hutchinson, A.L.; Cho, A.Y. Quantum cascade laser. *Science* **1994**, *264*, 553–556. [CrossRef]
2. Cheng, F.; Zhang, J.; Guan, Y.; Yang, P.; Zhuo, N.; Zhai, S.; Liu, J.; Wang, L.; Liu, S.; Liu, F.; et al. Ultralow power consumption of a quantum cascade laser operating in continuous-wave mode at room temperature. *Opt. Express* **2020**, *28*, 36497–36504. [CrossRef]
3. Wang, Z.; Kapsalidis, F.; Wang, R.; Beck, M.; Faist, J. Ultra-low threshold lasing through phase front engineering via a metallic circular aperture. *Nat. Commun.* **2022**, *13*, 230. [CrossRef]
4. Cheng, F.; Zhang, J.; Sun, Y.; Zhuo, N.; Zhai, S.; Liu, J.; Wang, L.; Liu, S.; Liu, F. High performance distributed feedback quantum cascade laser emitting at lambda approximately 6.12 um. *Opt. Express* **2022**, *30*, 5848–5854. [CrossRef] [PubMed]
5. Wang, H.; Zhang, J.; Cheng, F.; Zhuo, N.; Zhai, S.; Liu, J.; Wang, L.; Liu, S.; Liu, F.; Wang, Z. Watt-level, high wall plug efficiency, continuous-wave room temperature quantum cascade laser emitting at 7.7 microm. *Opt. Express* **2020**, *28*, 40155–40163. [CrossRef] [PubMed]
6. Fei, T.; Zhai, S.; Zhang, J.; Zhuo, N.; Liu, J.; Wang, L.; Liu, S.; Jia, Z.; Li, K.; Sun, Y.; et al. High power λ~8.5 µm quantum cascade laser grown by MOCVD operating continuous-wave up to 408 K. *J. Semicond.* **2021**, *42*, 112301. [CrossRef]
7. Botez, D.; Kirch, J.D.; Boyle, C.; Oresick, K.M.; Sigler, C.; Kim, H.; Knipfer, B.B.; Ryu, J.H.; Lindberg, D.; Earles, T.; et al. High-efficiency, high-power mid-infrared quantum cascade lasers [Invited]. *Opt. Mater. Express* **2018**, *8*, 1378. [CrossRef]
8. Bai, Y.; Bandyopadhyay, N.; Tsao, S.; Slivken, S.; Razeghi, M. Room temperature quantum cascade lasers with 27% wall plug efficiency. *Appl. Phys. Lett.* **2011**, *98*, 181102. [CrossRef]
9. Lyakh, A.; Suttinger, M.; Go, R.; Figueiredo, P.; Todi, A. 5.6 µm quantum cascade lasers based on a two-material active region composition with a room temperature wall-plug efficiency exceeding 28%. *Appl. Phys. Lett.* **2016**, *109*, 121109. [CrossRef]
10. Lu, Q.; Slivken, S.; Wu, D.; Razeghi, M. High power continuous wave operation of single mode quantum cascade lasers up to 5 W spanning lambda approximately 3.8–8.3 microm. *Opt. Express* **2020**, *28*, 15181–15188. [CrossRef]
11. Zhou, W.; Lu, Q.Y.; Wu, D.H.; Slivken, S.; Razeghi, M. High-power, continuous-wave, phase-locked quantum cascade laser arrays emitting at 8 microm. *Opt. Express* **2019**, *27*, 15776–15785. [CrossRef] [PubMed]
12. Spitz, O.; Didier, P.; Durupt, L.; Diaz-Thomas, D.A.; Baranov, A.N.; Cerutti, L.; Grillot, F. Free-space communication with directly modulated mid-infrared quantum cascade devices. *IEEE J. Sel. Top. Quantum Electron.* **2022**, *28*, 1–9. [CrossRef]
13. Dely, H.; Bonazzi, T.; Spitz, O.; Rodriguez, E.; Gacemi, D.; Todorov, Y.; Pantzas, K.; Beaudoin, G.; Sagnes, I.; Li, L.; et al. 10 Gbit s−1 free space data transmission at 9 µm wavelength with unipolar quantum optoelectronics. *Laser Photonics Rev.* **2021**, *16*, 2100414. [CrossRef]
14. Bismuto, A.; Terazzi, R.; Beck, M.; Faist, J. Influence of the growth temperature on the performances of strain-balanced quantum cascade lasers. *Appl. Phys. Lett.* **2011**, *98*, 091105. [CrossRef]
15. Razeghi, M.; Lu, Q.Y.; Bandyopadhyay, N.; Zhou, W.; Heydari, D.; Bai, Y.; Slivken, S. Quantum cascade lasers: From tool to product. *Opt. Express* **2015**, *23*, 8462–8475. [CrossRef] [PubMed]
16. Bai, Y.; Slivken, S.; Darvish, S.R.; Razeghi, M. Room temperature continuous wave operation of quantum cascade lasers with 12.5% wall plug efficiency. *Appl. Phys. Lett.* **2008**, *93*, 021103. [CrossRef]
17. Lyakh, A.; Maulini, R.; Tsekoun, A.; Go, R.; Pflügl, C.; Diehl, L.; Wang, Q.J.; Capasso, F.; Patel, C.K.N. 3 W continuous-wave room temperature single-facet emission from quantum cascade lasers based on nonresonant extraction design approach. *Appl. Phys. Lett.* **2009**, *95*, 141113. [CrossRef]
18. Lyakh, A.; Maulini, R.; Tsekoun, A.; Go, R.; Patel, C.K.N. Tapered 4.7 µm quantum cascade lasers with highly strained active region composition delivering over 4.5 watts of continuous wave optical power. *Opt. Express* **2012**, *20*, 4382–4388. [CrossRef]
19. Patel, C.K.N.; Troccoli, M.; Barron-Jimenez, R.; Titterton, D.H.; Grasso, R.J.; Richardson, M.A. Quantum cascade lasers: 25 years after the first demonstration. In Proceedings of the Technologies for Optical Countermeasures XVI, Strasbourg, France, 7 October 2019; SPIE: Washington, DC, USA, 2019; p. 1116102.
20. Zhijun, L.; Wasserman, D.; Howard, S.S.; Hoffman, A.J.; Gmachl, C.F.; Xiaojun, W.; Tanbun-Ek, T.; Liwei, C.; Fow-Sen, C. Room-temperature continuous-wave quantum cascade lasers grown by MOCVD without lateral regrowth. *IEEE Photonics Technol. Lett.* **2006**, *18*, 1347–1349. [CrossRef]
21. Lyakh, A.; Pflügl, C.; Diehl, L.; Wang, Q.J.; Capasso, F.; Wang, X.J.; Fan, J.Y.; Tanbun-Ek, T.; Maulini, R.; Tsekoun, A.; et al. 1.6W high wall plug efficiency, continuous-wave room temperature quantum cascade laser emitting at 4.6 µm. *Appl. Phys. Lett.* **2008**, *92*, 111110. [CrossRef]
22. Troccoli, M.; Diehl, L.; Bour, D.P.; Corzine, S.W.; Yu, N.; Wang, C.Y.; Belkin, M.A.; Hofler, G.; Lewicki, R.; Wysocki, G.; et al. High-Performance Quantum Cascade Lasers Grown by Metal-Organic Vapor Phase Epitaxy and Their Applications to Trace Gas Sensing. *J. Light. Technol.* **2008**, *26*, 3534–3555. [CrossRef]
23. Xie, F.; Caneau, C.; LeBlanc, H.P.; Visovsky, N.J.; Chaparala, S.C.; Deichmann, O.D.; Hughes, L.C.; Zah, C.-E.; Caffey, D.P.; Day, T. Room Temperature CW Operation of Short Wavelength Quantum Cascade Lasers Made of Strain Balanced $Ga_xIn_{1-x}As/Al_yIn_{1-y}As$ Material on InP Substrates. *IEEE J. Sel. Top. Quantum Electron.* **2011**, *17*, 1445–1452. [CrossRef]
24. Yao, Y.; Wang, X.; Fan, J.-Y.; Gmachl, C.F. High performance “continuum-to-continuum” quantum cascade lasers with a broad gain bandwidth of over 400 cm^{-1}. *Appl. Phys. Lett.* **2010**, *97*, 081115. [CrossRef]
25. Troccoli, M. High-Power Emission and Single-Mode Operation of Quantum Cascade Lasers for Industrial Applications. *IEEE J. Sel. Top. Quantum Electron.* **2015**, *21*, 61–67. [CrossRef]

26. Yang, Q.; Lösch, R.; Bronner, W.; Hugger, S.; Fuchs, F.; Aidam, R.; Wagner, J. High-peak-power strain-compensated GaInAs/AlInAs quantum cascade lasers (λ∼4.6 µm) based on a slightly diagonal active region design. *Appl. Phys. Lett.* **2008**, *93*, 251110. [CrossRef]
27. Sun, Y.; Yin, R.; Zhang, J.; Liu, J.; Fei, T.; Li, K.; Guo, K.; Jia, Z.; Liu, S.; Lu, Q.; et al. High-performance quantum cascade lasers at λ∼9 µm grown by MOCVD. *Opt. Express* **2022**, *30*, 37272. [CrossRef] [PubMed]
28. Bai, Y.; Bandyopadhyay, N.; Tsao, S.; Selcuk, E.; Slivken, S.; Razeghi, M. Highly temperature insensitive quantum cascade lasers. *Appl. Phys. Lett.* **2010**, *97*, 251104. [CrossRef]

Disclaimer/Publisher's Note: The statements, opinions and data contained in all publications are solely those of the individual author(s) and contributor(s) and not of MDPI and/or the editor(s). MDPI and/or the editor(s) disclaim responsibility for any injury to people or property resulting from any ideas, methods, instructions or products referred to in the content.